Article:
Mills, BJW, Belcher, CM, Lenton, TM et al. (2016) A modeling case for high atmospheric oxygen concentrations during the Mesozoic and Cenozoic. Geology, 44 (12). pp. 1023-1026. ISSN: 0091-7613

https://doi.org/10.1130/G38231.1

A modeling case for high atmospheric oxygen concentrations during the Mesozoic and Cenozoic

Benjamin J.W. Mills[1*], Claire M. Belcher[2], Timothy M. Lenton[2], and Robert J. Newton[1]

[1]*School of Earth and Environment, University of Leeds, Leeds LS2 9JT, UK*

[2]*College of Life and Environmental Sciences, University of Exeter, Exeter EX4 4QE, UK*

*E-mail: b.mills@leeds.ac.uk

ABSTRACT

Changes in atmospheric oxygen concentration over Earth history are commonly related to the evolution of animals and plants. But there is no direct geochemical proxy for O_2 levels, meaning that estimations rely heavily on modeling approaches. The results of such studies differ greatly, to the extent that today's atmospheric mixing ratio of 21% might be either the highest or lowest level during the past 200 m.y. Long term oxygen sources, such as the burial in sediments of reduced carbon and sulfur species, are calculated in models by representation of nutrient cycling and estimation of productivity, or by isotope mass balance (IMB)—a technique in which burial rates are inferred in order to match known isotope records. Studies utilizing these different techniques produce conflicting estimates for paleoatmospheric O_2, with nutrient-weathering models estimating concentrations close to, or above, that of the present day, and IMB models estimating low O_2, especially during the Mesozoic. Here we reassess the IMB technique using the COPSE biogeochemical model. IMB modelling is confirmed to be highly sensitive to assumed carbonate $\delta^{13}C$, and when this input is defined following recent

compilations, predicted O_2 is significantly higher and in reasonable agreement with that of non-IMB techniques. We conclude that there is no model-based support for low atmospheric oxygen concentrations during the past 200 m.y. High Mesozoic O_2 is consistent with wildfire records and the development of plant fire adaptions, but links between O_2 and mammal evolution appear more tenuous.

INTRODUCTION

Oxygen fuels the chemical reactions that take place in the mitochondria of eukaryotic cells, and pO_2 therefore places limits on the performance and survival of animals. Thus, changes in atmospheric O_2 concentration over Earth history are commonly seen as triggers for animal, and later for mammal, evolution (Lyons et al., 2014; Falkowski et al., 2005). Ratios of O_2:CO_2 determine the efficiency of photosynthesis, and variations in pO_2 dramatically influence wildfire dynamics, leading to strong potential links between pO_2 and plant evolution (He et al., 2012). But long-term variations in oxygen are difficult to estimate: the continuous presence of fossilized charcoal in sediments younger than 420 Ma indicates sufficient oxygen to sustain combustion (O_2 > 15% of the atmosphere, Belcher and McElwain, 2008), and the severity of fires in hyperoxic environments suggests that O_2 has remained below ~30% during this period (Jones and Chaloner, 1991; Belcher et al., 2010).

Between these limits, calculating variations in atmospheric oxygen relies on "forward" biogeochemical models of long-term O_2 source-and-sink processes or the interpretation of geochemical proxies (Fig. 1). Forward models can be divided into two groups, depending on how they estimate the burial rate of reduced carbon and sulfur, which are the principal sources of O_2 over geological time scales. These organically

mediated fluxes can be either estimated from the input of material and nutrients via weathering (Arvidson et al., 2013; Bergman et al., 2004; Hansen and Wallman, 2003; shown in green in Fig. 1) or inferred by comparing geological carbon and sulfur isotope records to the isotopic composition of modeled sediments (isotope mass balance [IMB]; Berner, 2009; Falkowski et al., 2005; red in Fig. 1).

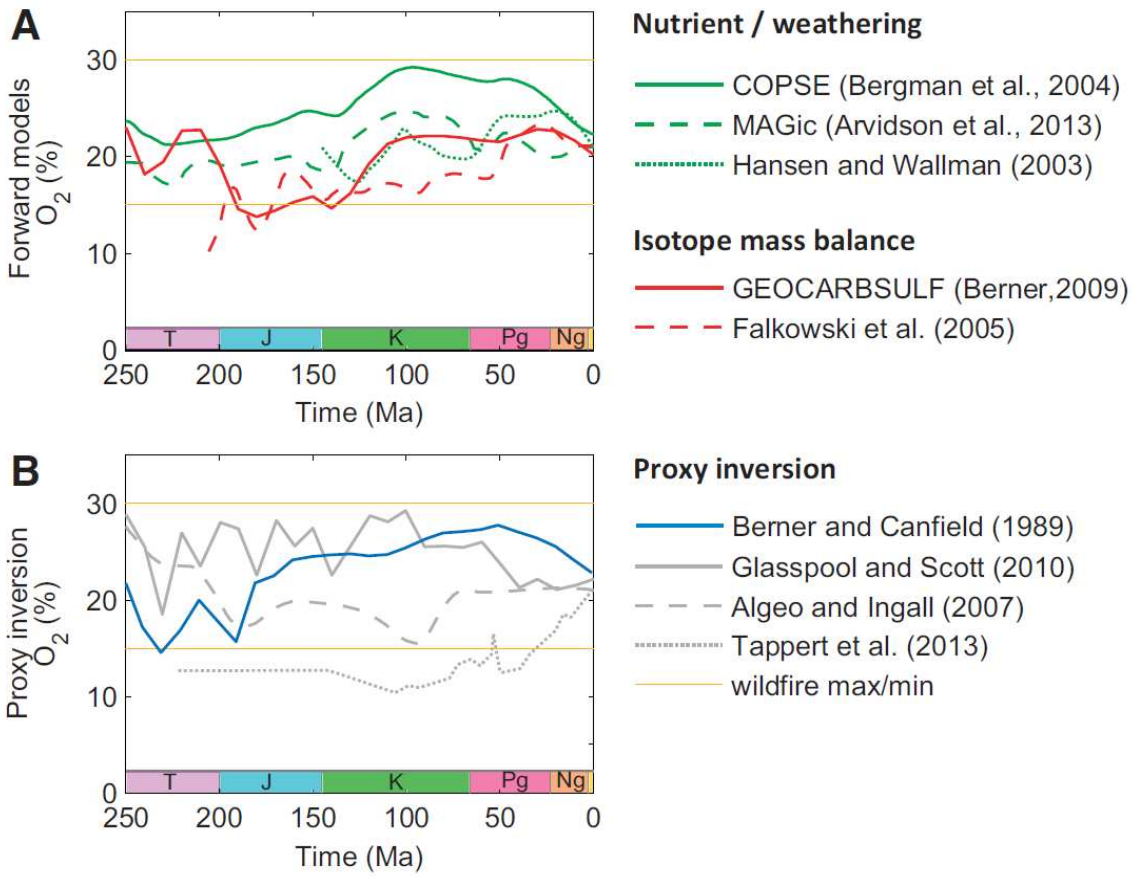

Figure 1. Reconstructions for Mesozoic and Cenozoic atmospheric O_2 mixing ratio. *A: Forward models of O_2 sources and sinks (green lines) and isotope mass balance models (red lines). B: Proxy inversion assuming relationships between O_2 concentration and either fossil charcoal abundance (Glasspool and Scott, 2010), carbon-to-phosphorus ratios in sediments (Algeo and Ingall, 2007), carbon isotope composition of plant resins (Tappert et al., 2013), or combined estimates for sedimentation rate and abundance of*

organic carbon and pyrite in rock samples (Berner and Canfield, 1989). Also shown: wildfire minimum and maximum (see text). T—Triassic; J—Jurassic; K—Cretaceous; Pg—Paleogene; Ng—Neogene.

Estimates of O_2 differ greatly between different forward models. Nutrient and weathering models typically predict higher values, while IMB models predict low pO_2 during the Mesozoic, potentially in conflict with the evidence for widespread fires (Belcher and McElwain, 2008). All models show general agreement for a gradual rise in pO_2 during the Cretaceous, although they disagree on whether this was a rise from low O_2 toward present values, or a rise from present to superambient levels, followed by a decline over the Cenozoic.

"Proxy inversion" methods estimate atmospheric oxygen by reference to geochemical data. Glasspool and Scott (2010) assumed a correlation between the abundance of charcoal in mires and atmospheric oxygen, scaling to the present-day value, and assumed a Permian-Carboniferous O_2 maximum of 30%. Algeo and Ingall (2007) related C_{org}:P (org—organic) ratios in organic-rich sediments to benthic redox conditions, and therefore to global atmospheric O_2 levels, scaling to the fire window. The "rock abundance" method of Berner and Canfield (1989) utilizes the carbon and sulfur contents of ancient sediments as well as sedimentation rate to infer oxygen production rates, linking this to pO_2. Tappert et al. (2013) inferred pO_2 from measured plant resin $\delta^{13}C$ and CO_2 proxies, reasoning that plant $\delta^{13}C$ reflects the CO_2:O_2 ratio of the growth environment. This technique produces very low estimates and is subject to high uncertainty in quantifying the plant $\delta^{13}C$ response to global O_2 and CO_2 variations.

The level of disagreement in current O_2 reconstructions is extreme and is masked to some degree by the scaling of many results to the fire window. This makes it difficult to assess the role of oxygen in the evolution of plants and animals during the Mesozoic and Cenozoic. Moreover, the forward models discussed here are commonly applied in studies of Paleozoic and Precambrian oxygen shifts (Clapham and Karr, 2012; Lenton and Watson, 2004), with important implications for the evolution of animals and land plants.

In this paper, we focus on the question of whether atmospheric oxygen concentration over the past 200 m.y. has been generally below or above the present-day value. We address this by exploring the isotope mass balance technique, which currently produces the most reliable and widely cited evidence for low Mesozoic oxygen.

FORWARD MODELING OF PALEOATMOSPHERIC OXYGEN CONCENTRATION

Forward models are based on the long-term carbon and sulfur cycles (e.g., Kump and Garrels, 1986), as shown in Figure 2. These systems consider atmospheric and oceanic carbon (*A*) and sulfur (*S*) and the much larger sedimentary reservoirs of oxidized and reduced species. The crustal reservoirs can be split into young (y) and ancient (a) sediments, with the assumption that the young reservoirs are smaller and constitute the majority of interaction with the surface system. This "rapid recycling" permits the isotopic signature of the young reservoirs to change more quickly and has a buffering effect when burial rates are calculated via isotope mass balance (Berner, 1987, 2009).

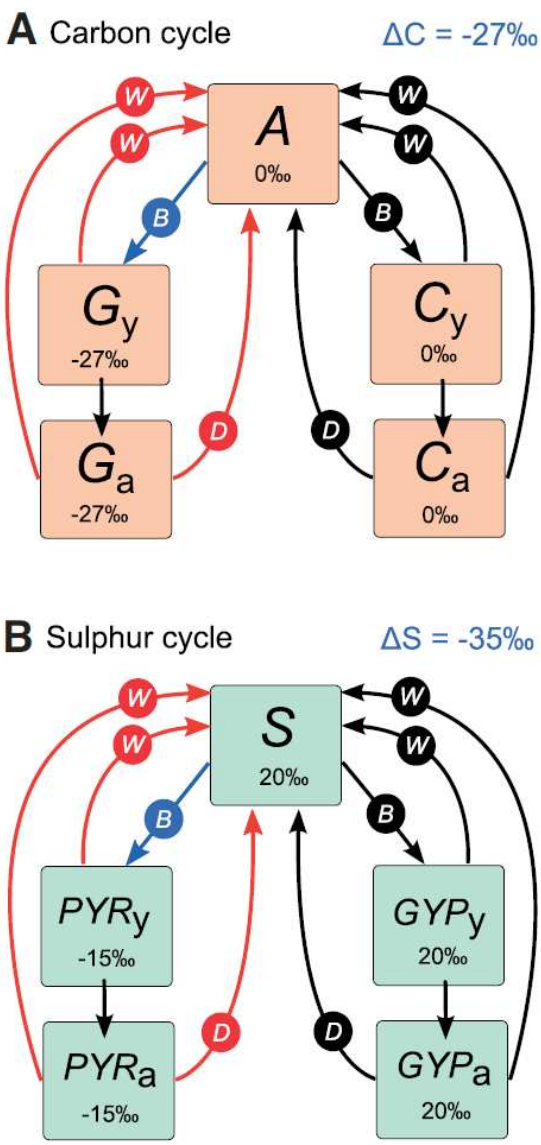

Figure 2. Long-term carbon and sulfur cycles. *Carbon cycle consists of fluxes between atmospheric and oceanic carbon (A), organic carbon (G), and carbonate (C). Sulfur cycle represents oceanic sulfate (S), buried pyrite (PYR), and gypsum (GYP). Burial (B) moves carbon and sulfur from the atmosphere and ocean to the crustal reservoirs, and it is returned by weathering (W) and degassing and metamorphism (D). Subscript "y" denotes young crustal reservoirs, "a" denotes ancient crustal reservoirs. Oxygen sources are shown in blue, sinks are shown in red. Other processes shown in black. Present-day isotope ratios $\delta^{13}C$ and $\delta^{34}S$ are shown for carbon and sulfur reservoirs respectively in per mil (‰); ΔC and ΔS show the burial fractionation effects for carbon and sulfur, respectively.*

Oxygen sources are the burial (*B*) of photosynthetically derived carbon and of pyrite sulfur (blue arrows in Fig. 2). Burial of these reduced species results in oxygenation of the surface environment. The buried species are eventually uplifted and

weathered (*W*) or are returned to the surface via metamorphism and degassing (*D*), which represent oxygen sinks (red in Fig. 2). The source-sink balance for O_2 is:

$$\frac{dO_2}{dt} = B(G) - W(G_y) - W(G_a) - D(G_a) + 2\left[B(PYR) - W(PYR_y) - W(PYR_a) - D(PYR_a)\right], \quad (1)$$

where *G* is organic carbon and *PYR* is buried pyrite.

Models calculate these fluxes, informed by internal parameters such as temperature, rates of erosion and degassing, rock exposure, and biological processes (Berner, 2006; Bergman et al., 2004). Burial, weathering, and degassing of the oxidized forms of carbon and sulfur (black arrows in Fig. 2) do not impact oxygen concentration directly but do affect the size and isotopic composition of the surface reservoirs (*A*, *S*), so cannot be ignored.

Isotope Mass Balance

Organic carbon and pyrite sulfur are isotopically lighter than the CO_2 and SO_4 they are derived from, due to kinetic selection during photosynthesis and sulfate reduction. The canonical isotope ratios for the present-day system (Hayes et al., 1999) are shown in Figure 2, alongside the fractionation effects ΔC (carbon) and ΔS (sulfur). These isotopic compositions and fractionation effects have changed over Earth history. For example, increasing the burial rate of organic, isotopically depleted carbon would act to increase the isotope ratio $\delta^{13}C$ in the parent surface reservoir *A*.

Assuming that buried carbonates and sulfates reflect ancient oceanic isotopic composition, the geological $\delta^{13}C$ and $\delta^{34}S$ records can be used to back-calculate the required rate of burial of organic carbon and pyrite sulfur and therefore the rate of oxygen production (Berner, 1987). This requires knowledge of the input fluxes via weathering

147 and degassing (W, D), the isotopic composition of the crustal reservoirs, and the
148 fractionation effects ΔC and ΔS. The isotope mass balance equations consider isotopic
149 inputs and outputs and are rearranged to calculate burial rates. The mass balance for the
150 carbon system is shown below, and the sulfur system follows the same structure. See
151 Berner (1987) and Berner (2001) for detailed descriptions. Here δ(X) is the isotopic
152 composition of reservoir X:

153 $$B(G) = \frac{1}{\Delta C}\{[\delta(A) - \delta(G_y)]W(G_y) + [\delta(A) - \delta(G_a)][W(G_a) + D(G_a)] +$$

154 $$[\delta(A) - \delta(C_y)]W(C_y) + [\delta(A) - \delta(C_a)][W(C_a) + D(C_a)]\} . \quad (2)$$

155 The GEOCARBSULF model (Berner, 2006, 2009; Fig. 1A) combines the isotope
156 mass balance technique with calculations for biogeochemical carbon and sulfur fluxes,
157 and is generally considered the current "best-guess" atmospheric O_2 prediction. Error
158 analysis of the GEOCARBSULF model (Royer et al., 2014) plots model predictions for
159 variation in all input parameters and robustly predicts low Mesozoic O_2. However, this
160 study is hampered by high model failure rate (the model crashes when some inputs are
161 changed significantly from their default values), allowing only minimal variation of the
162 $\delta^{13}C$ input [$\delta(A)$ in Equation 2], far from the uncertainty in global records.

163 **The IMB-COPSE Model**

164 We re-evaluate the oxygen predictions via isotope mass using the revised COPSE
165 model (Mills et al., 2014). COPSE is a derivative of the GEOCARB models and uses
166 many of the same calculations, but it differs from GEOCARBSULF in several ways that
167 make it potentially more useful for evaluating O_2 predictions: the model is solved
168 numerically using an implicit variable order method (Shampine and Reichelt, 1997),
169 which greatly reduces model failure rate and allows testing of different $\delta^{13}C$ inputs. The

model also integrates recent research on the global rate of CO_2 degassing and the weathering of volcanic rocks (Van Der Meer et al., 2014; Mills et al., 2014), which has not previously been applied to oxygen calculation.

The standard COPSE model includes nutrient cycles in order to estimate productivity and calculate the fluxes of organic carbon and pyrite sulfur burial. In this exploration (IMB-COPSE), the nutrient cycles are removed and the productivity and burial calculations are replaced with the standard isotope mass balance equations (Berner, 2001; Equation 2), following their incorporation into GEOCARBSULF (Berner, 2006). This includes the addition of rapid recycling. See the GSA Data Repository[1] for full model description.

MODEL INPUTS AND RESULTS

Initially the IMB-COPSE model is run using the GEOCARBSULF $\delta^{13}C$ and $\delta^{34}S$ inputs (red dashed line in Fig. 3A). Despite the differences in model weathering and degassing processes, the IMB-COPSE model produces O_2 predictions that are strikingly similar to those of GEOCARBSULF (black and red lines in Fig. 3B). This includes a prolonged period of low atmospheric O_2 during the Jurassic and Early Cretaceous.

We explore model sensitivity to assumed $\delta^{13}C$ and $\delta^{34}S$ records by removing the GEOCARBSULF inputs and replacing them with values from recent literature compilations. Current records for Phanerozoic $\delta^{34}S$ (Algeo et al., 2015) do not differ greatly from the GEOCARBSULF inputs, and their substitution has little impact on model predictions (see the Data Repository). Recent compilations of carbonate $\delta^{13}C$, however, show notable differences from the curves used in GEOCARBSULF.

192 The $\delta^{13}C$ compilation of Saltzman and Thomas (2012; denoted GTS2012) is
193 shown in blue in Figure 3A. The solid line shows the moving average, and dashed lines
194 show $\pm 1\sigma$ over 5 m.y. bins. The Mesozoic record is at higher resolution than the
195 GEOCARBSULF input but does not show substantial base-level differences. The
196 GTS2012 curve incorporates recent Cenozoic data from benthic foraminifera (Cramer et
197 al., 2009), which agrees with the bulk record of $\delta^{13}C$ in pelagic carbonates (Katz et al.,
198 2005) in giving a present-day oceanic $\delta^{13}C$ value close to 0‰, whereas the
199 GEOCARBSULF curve has a present-day value closer to 2‰. This value is extremely
200 important in isotope mass balance modeling as it sets the relative state of the system as
201 we explore ancient time periods. During the Jurassic period, the GEOCARBSULF curve
202 assumes a global ocean $\delta^{13}C$ signature that is isotopically lighter than at present,
203 potentially indicative of lower organic carbon burial and less oxygen production. The
204 GTS2012 curve, however, shows a generally heavier signal than at present.
205 These differences in assumed oceanic $\delta^{13}C$ translate into large differences in
206 model O_2 predictions, which tend to follow this input qualitatively. Under the GTS2012
207 input, the average predicted O_2 concentration (blue in Fig. 3B) remains at or above
208 present values during the past 200 m.y., resolving the conflict with nutrient- and
209 weathering-based models and with the wildfire minimum. Note that the O_2 predictions
210 for the $\pm 1\sigma$ $\delta^{13}C$ inputs cross each other due to the present-day O_2 constraint. See the
211 Data Repository for further model uncertainty estimates, including constraints on the
212 sulfur cycle.
213

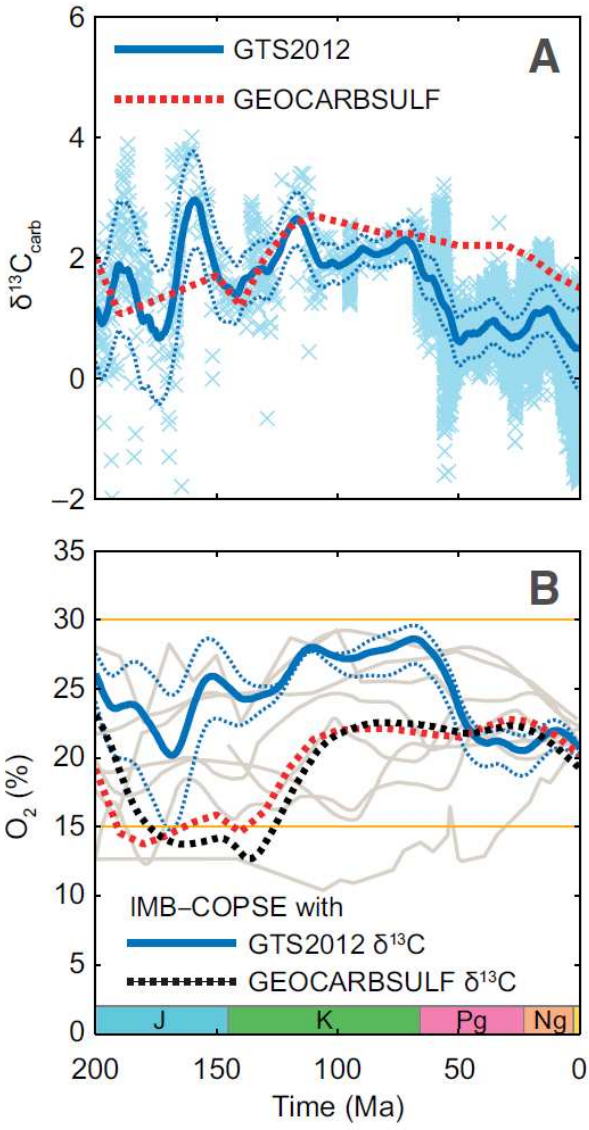

Figure 3. Results of isotope mass balance (IMB)-COPSE model. *A: $\delta^{13}C$ input follows Geological Time Scale 2012 (GTS2012) (Saltzman and Thomas, 2012; blue; crosses show data points, solid line shows moving average, and dashed lines show ±1σ) or GEOCARBSULF model (Berner, 2009; red). B: Oxygen mixing ratios (%) predicted by IMB-COPSE model given $\delta^{13}C$ input from GTS2012 (blue) or GEOCARBSULF (black dashed), compared to GEOCARBSULF O_2 output (red). Estimates from Figure 1 shown in gray, with fire window in orange. For full model output see Data Repository (see footnote 1). J—Jurassic; K—Cretaceous; Pg—Paleogene; Ng—Neogene.*

DISCUSSION

Examination of IMB modeling confirms that the predicted rate of burial of organic carbon (the largest source of O_2) is heavily dependent on the assumed carbon

236 isotope record and much less dependent on other model processes, meaning that
237 assumptions about the variation in oceanic $\delta^{13}C$ are critical in determining pO_2.
238 Compiling the global record of average whole-ocean $\delta^{13}C$ is difficult, as
239 differences exist across species, depth, and temperature (Saltzman and Thomas, 2012;
240 Cramer et al., 2009). The paleogeographic source of information at different times adds
241 further uncertainty: in sediments older than the Early Cretaceous the majority of records
242 are sourced from epeiric seas rather than open-ocean margins or the deep ocean. A
243 variety of studies have shown that ancient epeiric-sea water masses could develop
244 isotopic signatures distinct from those of the open ocean for a number of isotope systems
245 including carbon (Coulson et al., 2011; Panchuk et al., 2006; Newton et al., 2011).
246 These sources of uncertainty and variability lead to significant uncertainty in the
247 overall curve, and crucially, in whether the present-day value is lower or higher than
248 average values over the Mesozoic and Cenozoic. Current GEOCARBSULF model
249 predictions of low Mesozoic pO_2 rely on the assumption that modern oceanic $\delta^{13}C$ values
250 are higher than those during the Mesozoic, which is not shown in recent records based on
251 either bulk-rock (Katz et al., 2005) or single-organism (Cramer et al., 2009) compilations.
252 We therefore conclude that there is no model-based support for low Mesozoic pO_2
253 concentrations.
254 Taking our results together with the forward modeling approaches that calculate
255 oxygen production via weathering and nutrient systems (Fig. 1), we argue for high O_2
256 during the Mesozoic and Cenozoic, with a rise to above-modern oxygen concentrations
257 during the Cretaceous. This view is compatible with the limits of combustion (Belcher
258 and McElwain, 2008). Low-oxygen predictions are not a necessary consequence of

isotope mass balance modeling, while estimations based on the $\delta^{13}C$ composition of plant material (Tappert et al., 2013) are extremely difficult to validate due to the high variability of measured values and absence of controlled growth experiments in different CO_2:O_2 ratios.

Linking variations in oxygen concentration to animal evolution is speculative, and it is difficult to separate ecological and climatic drivers (Smith et al., 2010; Clapham and Karr, 2012). Proxies for O_2 based on plant flammability are useful, but must be expanded to consider linkages between pO_2 and fire-adapted trait selection (e.g., He et al., 2012, 2015; Lamont and Downes, 2011). Reconstructing atmospheric oxygen via modeling studies depends greatly on the ability to accurately compile average, whole-ocean $\delta^{13}C$ for the ancient past, whether this record is used to directly drive the model (IMB) or as a means of comparison to model outputs. It is clear that modelers and paleontologists should seek to work together if we are to better explore the links between oxygen and evolution.

ACKNOWLEDGMENTS

We thank the late R.A. Berner for the GEOCARBSULF model code, and M.R. Saltzman and E. Thomas for isotope data. Mills is funded by a University of Leeds Academic Fellowship; Belcher acknowledges funding from European Research Council Starter Grant ERC-2013-StG-335891-ECOFLAM. Lenton acknowledges funding from the Leverhulme Trust (RPG-2013-106). We thank Noah Planavsky and two anonymous reviewers for assessing this work.

REFERENCES CITED

281 Algeo, T.J., and Ingall, E., 2007, Sedimentary C_{org}:P ratios, paleocean ventilation, and
282 Phanerozoic atmospheric pO_2: Palaeogeography, Palaeoclimatology, Palaeoecology,
283 v. 256, p. 130–155, doi:10.1016/j.palaeo.2007.02.029.
284 Algeo, T.J., Luo, G.M., Song, H.Y., Lyons, T.W., and Canfield, D.E., 2015,
285 Reconstruction of secular variation in seawater sulfate concentrations:
286 Biogeosciences, v. 12, p. 2131–2151, doi:10.5194/bg-12-2131-2015.
287 Arvidson, R.S., Mackenzie, F.T., and Guidry, M.W., 2013, Geologic history of seawater:
288 A *MAGic* approach to carbon chemistry and ocean ventilation: Chemical Geology,
289 v. 362, p. 287–304, doi:10.1016/j.chemgeo.2013.10.012.
290 Belcher, C.M., and McElwain, J.C., 2008, Limits for combustion in low O_2 redefine
291 paleoatmospheric predictions for the Mesozoic: Science, v. 321, p. 1197–1200,
292 doi:10.1126/science.1160978.
293 Belcher, C.M., Yearsley, J.M., Hadden, R.M., McElwain, J.C., and Rein, G., 2010,
294 Baseline intrinsic flammability of Earth's ecosystems estimated from
295 paleoatmospheric oxygen over the past 350 million years: Proceedings of the
296 National Academy of Sciences of the United States of America, v. 107, p. 22,448–
297 22,453, doi:10.1073/pnas.1011974107.
298 Bergman, N.M., Lenton, T.M., and Watson, A.J., 2004, COPSE: A new model of
299 biogeochemical cycling over Phanerozoic time: American Journal of Science, v. 304,
300 p. 397–437, doi:10.2475/ajs.304.5.397.
301 Berner, R.A., 1987, Models for carbon and sulfur cycles and atmospheric oxygen:
302 Application to Paleozoic geologic history: American Journal of Science, v. 287,
303 p. 177–196, doi:10.2475/ajs.287.3.177.

304 Berner, R.A., 2001, Modelling atmospheric O_2 over Phanerozoic time: Geochimica et
305 Cosmochimica Acta, v. 65, p. 685–694, doi:10.1016/S0016-7037(00)00572-X.
306 Berner, R.A., 2006, GEOCARBSULF: A combined model for Phanerozoic atmospheric
307 O_2 and CO_2: Geochimica et Cosmochimica Acta, v. 70, p. 5653–5664,
308 doi:10.1016/j.gca.2005.11.032.
309 Berner, R.A., 2009, Phanerozoic atmospheric oxygen: New results using the
310 GEOCARBSULF model: American Journal of Science, v. 309, p. 603–606,
311 doi:10.2475/07.2009.03.
312 Berner, R.A., and Canfield, D.E., 1989, A new model for atmospheric oxygen over
313 Phanerozoic time: American Journal of Science, v. 289, p. 333–361,
314 doi:10.2475/ajs.289.4.333.
315 Clapham, M.E., and Karr, J.A., 2012, Environmental and biotic controls on the
316 evolutionary history of insect body size: Proceedings of the National Academy of
317 Sciences of the United States of America, v. 109, p. 10,927–10,930,
318 doi:10.1073/pnas.1204026109.
319 Coulson, A.B., Kohn, M.J., and Barrick, R.E., 2011, Isotopic evaluation of ocean
320 circulation in the Late Cretaceous North American seaway: Nature Geoscience, v. 4,
321 p. 852–855, doi:10.1038/ngeo1312.
322 Cramer, B.S., Toggweiler, J.R., Wright, J.D., Katz, M.E., and Miller, K.G., 2009, Ocean
323 overturning since the Late Cretaceous: Inferences from a new benthic foraminiferal
324 isotope compilation: Paleoceanography, v. 24, PA4216, doi:10.1029/2008PA001683.
325 Falkowski, P.G., Katz, M.E., Milligan, A.J., Fennel, K., Cramer, B.S., Aubry, M.P.,
326 Berner, R.A., Novacek, M.J., and Zapol, W.M., 2005, The rise of oxygen over the

past 205 million years and the evolution of large placental mammals: Science, v. 309, p. 2202–2204, doi:10.1126/science.1116047.

Glasspool, I.J., and Scott, A.C., 2010, Phanerozoic concentrations of atmospheric oxygen reconstructed from sedimentary charcoal: Nature Geoscience, v. 3, p. 627–630, doi:10.1038/ngeo923.

Hansen, K.W., and Wallman, K., 2003, Cretaceous and Cenozoic evolution of seawater composition, atmospheric O_2 and CO_2: A model perspective: American Journal of Science, v. 303, p. 94–148, doi:10.2475/ajs.303.2.94.

Hayes, J.M., Strauss, H., and Kaufman, A.J., 1999, The abundance of ^{13}C in marine organic matter and isotopic fractionation in the global biogeochemical cycle of carbon during the past 800 Ma: Chemical Geology, v. 161, p. 103–125, doi:10.1016/S0009-2541(99)00083-2.

He, T., Pausas, J.G., Belcher, C.M., Schwilk, D.W., and Lamont, B.B., 2012, Fire-adapted traits of *Pinus* arose in the fiery Cretaceous: The New Phytologist, v. 194, p. 751–759, doi:10.1111/j.1469-8137.2012.04079.x.

He, T., Belcher, C.M., Lamont, B.B., and Lim, S.L., 2015, A 350-million-year legacy of fire adaption among conifers: Journal of Ecology, v. 104, p. 352–363, doi:10.1111/1365-2745.12513.

Jones, T., and Chaloner, W., 1991, Fossil charcoal, its recognition and palaeoatmospheric significance: Palaeogeography, Palaeoclimatology, Palaeoecology, v. 97, p. 39–50, doi:10.1016/0031-0182(91)90180-Y.

348 Katz, M.E., Wright, J.D., Miller, K.G., Cramer, B.S., Fennel, K., and Falkowski, P.G.,
349 2005, Biological overprint of the geological carbon cycle: Marine Geology, v. 217,
350 p. 323–338, doi:10.1016/j.margeo.2004.08.005.
351 Kump, L.R., and Garrels, R.M., 1986, Modeling atmospheric O_2 in the global
352 sedimentary redox cycle: American Journal of Science, v. 286, p. 337–360,
353 doi:10.2475/ajs.286.5.337.
354 Lamont, B.B., and Downes, S., 2011, Fire-stimulated flowering among resprouters and
355 geophytes in Australia and South Africa: Plant Ecology, v. 212, p. 2111–2125,
356 doi:10.1007/s11258-011-9987-y.
357 Lenton, T.M., and Watson, A.J., 2004, Biotic enhancement of weathering, atmospheric
358 oxygen and carbon dioxide in the Neoproterozoic: Geophysical Research Letters,
359 v. 31, L05202, doi:10.1029/2003GL018802.
360 Lyons, T.W., Reinhard, C.T., and Planavsky, N.J., 2014, The rise of oxygen in Earth's
361 early ocean and atmosphere: Nature, v. 506, p. 307–315, doi:10.1038/nature13068.
362 Mills, B., Daines, S.J., and Lenton, T.M., 2014, Changing tectonic controls on the long-
363 term carbon cycle from Mesozoic to present: Geochemistry Geophysics Geosystems,
364 v. 15, p. 4866–4884, doi:10.1002/2014GC005530.
365 Newton, R.J., Reeves, E.P., Kafousia, N., Wignall, P.B., Bottrell, S.H., and Sha, J.G.,
366 2011, Low marine sulfate concentrations and the isolation of the European
367 epicontinental sea during the Early Jurassic: Geology, v. 39, p. 7–10,
368 doi:10.1130/G31326.1.
369 Panchuk, K.M., Holmden, C.E., and Leslie, S.A., 2006, Local controls on carbon cycling
370 in the Ordovician midcontinent region of North America, with implications for

carbon isotope secular curves: Journal of Sedimentary Research, v. 76, p. 200–211, doi:10.2110/jsr.2006.017.

Royer, D.L., Donnadieu, Y., Park, J., Kowalczyk, J., and Godderis, Y., 2014, Error analysis of CO_2 and O_2 estimates from the long-term geochemical model GEOCARBSULF: American Journal of Science, v. 314, p. 1259–1283, doi:10.2475/09.2014.01.

Saltzman, M.R., and Thomas, E., 2012, Carbon isotope stratigraphy, *in* Gradstein, F.M., et al., eds., The Geological Time Scale 2012: Boston, Elsevier, p. 207–232, doi:10.1016/B978-0-444-59425-9.00011-1.

Shampine, L.F., and Reichelt, M.W., 1997, The MATLAB ODE suite: SIAM Journal on Scientific Computing, v. 18, p. 1–22, doi:10.1137/S1064827594276424.

Smith, F.A., et al., 2010, The evolution of maximum body size of terrestrial mammals: Science, v. 330, p. 1216–1219, doi:10.1126/science.1194830.

Tappert, R., McKellar, R.C., Wolfe, A.P., Tappert, M.C., Ortega-Blanco, J., and Muehlenbachs, K., 2013, Stable carbon isotopes of C_3 plant resins and ambers record changes in atmospheric oxygen since the Triassic: Geochimica et Cosmochimica Acta, v. 121, p. 240–262, doi:10.1016/j.gca.2013.07.011.

Van Der Meer, D.G., Zeebe, R.E., Hinsbergen, D.J.J.V., Sluijs, A., Spakman, W., and Torsvik, T.H., 2014, Plate tectonic controls on atmospheric CO_2 levels since the Triassic: Proceedings of the National Academy of Sciences of the United States of America, v. 111, p. 4380–4385, doi:10.1073/pnas.1315657111.

[1]GSA Data Repository item 2016xxx, is available online at http://www.geosociety.org/pubs/ft2016.htm or on request from editing@geosociety.org.

Mills_2016_O2.xlsx: Datafile of oxygen reconstructions from the IMB-COPSE model.

APPENDIX

APPENDIX 1: ALTERATIONS TO PREVIOUSLY PUBLISHED MODEL

The COPSE and GEOCARB models

The original COPSE model (Bergman et al., 2004) is a long term biogeochemical box model, based on the GEOCARB models (Berner 1991, 1994, Berner and Kothavala, 2001). It calculates fluxes between the atmosphere/ocean and sedimentary reservoirs of oxidised and reduced carbon and sulphur to estimate changes in CO_2, O_2 and ocean sulphate over the Phanerozoic. Since publication of COPSE, GEOCARB has been extended to include calculations for the sulphur cycle and oxygen (GEOCARBSULF). In Mills et al. (2014), COPSE was updated to consider the weatherable area of different rock types, and to investigate alternative reconstructions for volcanic degassing rates (Van Der Meer et al., 2014). The model predictions were compared to variation in seawater $^{87}Sr/^{86}Sr$.

The critical difference between COPSE and GEOCARBSULF is the method used to estimate the burial rates of organic carbon and pyrite sulphur, which are the long term sources of oxygen. COPSE uses integrated cycles of limiting nutrients P and N (following Lenton and Watson 2000) to estimate these fluxes based on other model parameters, such as nutrient delivery via weathering. GEOCARBSULF uses an isotope mass balance technique (IMB: Berner 1987, 2001) which infers the burial rates from

416 known changes in isotope ratios $\delta^{13}C$ and $\delta^{34}S$, and does not require the calculation of
417 nutrient fluxes. Whist model predictions for CO_2 over the Phanerozoic are broadly
418 similar, predictions for variation in O_2 are substantially different.
419
420 **Model used in this work**
421 This paper uses the latest version of the COPSE biogeochemical model (Mills et
422 al., 2014), and adds to this a routine for calculating the burial rates of organic carbon and
423 pyrite sulphur via isotope mass balance, mirroring the functionality of the
424 GEOCARBSULF model (Berner, 2006; 2009). The resulting model is very similar to
425 GEOCARBSULF, but differences remain in the assumed rate of volcanic degassing, and
426 the weatherable area of volcanic rocks, as well as more minor quantitative differences in
427 the calculations for weathering fluxes.
428 In this paper we wish to test the oxygen predictions from the isotope mass balance
429 system, particularly with regard to the input of $\delta^{13}C$ data, which shows large uncertainty.
430 In theory, this test can be carried out using the GEOCARBSULF model, however recent
431 work has shown that the computational algorithm used to solve the model fails when $\delta^{13}C$
432 inputs are varied only slightly from the model baseline (Royer et al., 2014). The COPSE
433 algorithm uses a variable time-step method and is therefore suited to testing wide
434 differences in input parameters. Thus we adapt the COPSE model to test the isotope mass
435 balance method by removing the nutrient system and replacing with the IMB equations.
436 This has the additional benefit of testing whether the differences in the COPSE
437 formulations for degassing and weathering have much impact on the model outputs under
438 isotope mass balance.

To summarize the results of this exercise:

- Replacing the nutrient system in COPSE with the exact isotope mass balance system from GEOCARBSULF (including standard inputs for $\delta^{13}C$ and $\delta^{34}S$) results in oxygen predictions very similar to GEOCARBSULF. Showing that O_2 predictions are much more dependent on the assumed isotope record than other model processes.
- Replacing the standard $\delta^{13}C$ input compilation with a more recent record (Saltzman and Thomas, 2012) results in major revision of the O_2 predictions, with $pO_2 > 0.2atm$ for the whole model timeframe (200-0Ma).

Rapid recycling

In order to add the isotope mass balance system to COPSE, the model must be modified to include 'rapid recycling' of sedimentary carbon and sulphur. Under this method, it is assumed that geologically young sedimentary rocks constitute the majority of interaction with the surface system, allowing the isotopic signature of buried material to be more quickly recycled to the atmosphere and oceans. This technique has been included in all isotope mass balance approaches (Berner 1987; 2006; 2009; Royer et al., 2014).

The method involves splitting the sedimentary reservoirs for organic carbon, carbonates, pyrite and gypsum sulphur into 'young' and 'ancient' boxes. The young boxes are smaller and have higher weathering rates, the ancient boxes are much larger and have lower weathering rates (see ms figure 2). The relative size of the young and ancient reservoirs, as well as the relative weathering contributions are taken directly from

GEOCARBSULF, and are listed below with the other model parameters. The carbon and sulphur cycle schematic from the attached manuscript, which details the flux names, is reproduced here (A1) for convenience.

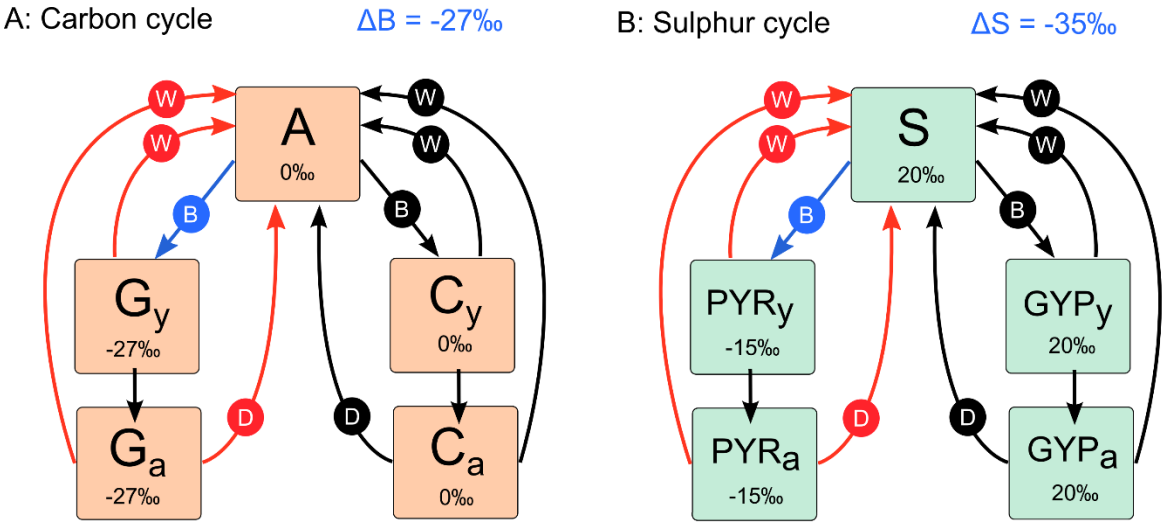

Figure A1. Long term carbon and sulphur cycles. The carbon cycle consists of fluxes between atmosphere and ocean carbon (A), organic carbon (G) and carbonate (C). The sulphur cycle represents ocean sulphate (S), buried reduced pyrite (PYR) and oxidised gypsum (GYP). Burial (B) moves carbon and sulphur from the atmosphere and ocean to the crustal reservoirs, and it is returned by weathering (W) and degassing/metamorphism (D). Subscript (y) denotes young crustal reservoirs, (a) denotes ancient crustal reservoirs. Oxygen sources are shown in blue, sinks are shown in red. Present day isotope ratios $\delta^{13}C$ and $\delta^{34}S$ are shown for carbon and sulphur reservoirs respectively in per mil (‰), ΔB and ΔS show the burial fractionation effects for carbon and sulphur respectively.

Isotope mass balance equations for burial fluxes

With rapid recycling added to the COPSE model, and the nutrient system removed completely, the equations representing organic carbon burial and pyrite sulphur burial are copied exactly from GEOCARBSULF, the code for which was kindly sent by R. A. Berner. The mathematical derivation is published in Berner (1987) and begins with the assumption of input-output parity for ^{12}C and ^{13}C atoms (and ^{34}S and ^{32}S for sulphur). For Carbon:

$$Input \times \delta(Input) = Output \times \delta(Output) \quad (1)$$

$$W(G_y)\delta(G_y) + W(G_a)\delta(G_a) + D(G_a)\delta(G_a) + W(C_y)\delta(C_y) + W(C_a)\delta(C_a) + D(C_a)\delta(C_a) = B(G)(\delta(A) - \Delta B) + B(C)\delta(A) \quad (2)$$

Rearranging gives:

$$\Delta B \times B(G) = \left(\delta(A) - \delta(G_y)\right) W(G_y) + \left(\delta(A) - \delta(G_a)\right)\left(W(G_a) + D(G_a)\right) + \left(\delta(A) - \delta(C_y)\right)W(C_y) + \left(\delta(A) - \delta(C_a)\right)\left(W(C_a) + D(C_a)\right) \quad (3)$$

Where δ(X) is the isotopic composition of reservoir X, W denotes weathering, D denotes degassing and B denotes burial. ΔB and ΔS are the fractionation effects for burial of carbon and sulphur respectively. This equation is mirrored for the sulphur cycle.

APPENDIX 2: FULL MODEL DESCRIPTION

The full model equations are detailed below. Aside from the addition of rapid recycling and isotope mass balance, and the removal of the nutrient system, they follow

exactly the model from Mills et al., (2014). The flux names from the manuscript are simplified here for convenience:

$W(C_y) = carbw_y, W(C_a) = carbw_a, W(G_y) = oxidw_y, W(G_a) = oxidw_a,$

$D(C) = ccdeg, D(G) = ocdeg, B(G) = ocb, B(C) = mccb$

$W(GYP_y) = gypw_y, W(GYP_a) = gypw_a, W(PYR_y) = pyrw_y, W(PYR_a) = pyrw_a,$

$D(GYP) = gypdeg, D(PYR) = pyrdeg, B(GYP) = mgsb, B(PYR) = mpsb$

Reservoir calculations:

Atmosphere/ocean carbon:

$$\frac{dA}{dt} = ccdeg + carbw_y + carbw_a + oxidw_y + oxidw_a + ocdeg$$
$$-mccb - ocb - sfw \quad (4)$$

Ocean sulphate:

$$\frac{dS}{dt} = pyrw_y + pyrw_a + pyrdeg + gypw_y + gypw_y + gypdeg$$
$$-mpsb - mgsb \quad (5)$$

Buried organic C (young): $\frac{dG_y}{dt} = ocb - oxidw_y - F_{Gya}$ (6)

Buried organic C (ancient): $\frac{dG_a}{dt} = F_{Gya} - oxidw_a - ocdeg$ (7)

Buried carbonate C (young): $\frac{dC_y}{dt} = mccb - carbw_y - F_{Cya}$ (8)

Buried carbonate C (ancient): $\frac{dC_a}{dt} = F_{Cya} - carbw_a - ccdeg$

(9)

Buried pyrite S (young): $\frac{dPYR_y}{dt} = mpsb - pyrw_y - F_{PYRya}$

(10)

Buried pyrite S (ancient): $\frac{dPYR_a}{dt} = F_{PYRya} - pyrw_a - pyrdeg$

(11)

Buried gypsum S (young): $\frac{dGYP_y}{dt} = mgsb - gypw_y - F_{GYPya}$

(12)

Buried gypsum S (ancient): $\frac{dGYP_a}{dt} = F_{GYPya} - gypw_a - gypdeg$

(13)

Isotope reservoir calculations:

Atmosphere/ocean carbon:

$$\frac{d(A\times\delta(A))}{dt} = ccdeg \times \delta(C_a) + carbw_y \times \delta(C_y) + carbw_a \times \delta(C_a) + oxidw_y \times \delta(G_y) + oxidw_a \times \delta(G_a) + ocdeg \times \delta(G_a) - ocb \times (\delta(A) - \Delta B) - mccb \times \delta(A) - sfw \times \delta(A)$$

(14)

Ocean sulphate:

$$\frac{d(S\times\delta(S))}{dt} = gypdeg \times \delta(GYP_a) + gypw_y \times \delta(GYP_y) + gypw_a \times \delta(GYP_a) + pyrw_y \times \delta(PYR_y) + pyrw_a \times \delta(PYR_a) + pyrdeg \times \delta(PYR_a) - mpsb \times (\delta(S) - \Delta S) - mgsb \times \delta(S)$$

(15)

Buried organic C (young):

$$\frac{d(G_y \times \delta(G_y))}{dt} = ocb \times (\delta(A) - \Delta B) - oxidw_y \times \delta(G_y) - F_{Gya} \times \delta(G_y) \quad (16)$$

Buried organic C (ancient):

$$\frac{d(G_a \times \delta(G_a))}{dt} = F_{Gya} \times \delta(G_y) - oxidw_a \times \delta(G_a) - ocdeg \times \delta(G_a) \quad (17)$$

Buried carbonate C (young):

$$\frac{d(C_y \times \delta(C_y))}{dt} = mccb \times \delta(A) - carbw_y \times \delta(C_y) - F_{Cya} \times \delta(C_y) \quad (18)$$

Buried carbonate C (ancient):

$$\frac{d(C_a \times \delta(C_a))}{dt} = F_{Cya} \times \delta(C_y) - carbw_a \times \delta(C_a) - ccdeg \times \delta(C_a) \quad (19)$$

Buried pyrite S (young):

$$\frac{d(PYR_y \times \delta(PYR_y))}{dt} = mpsb \times (\delta(S) - \Delta S) - pyrw_y \times \delta(PYR_y) - F_{PYRya} \times \delta(PYR_y) \quad (20)$$

Buried pyrite S (ancient):

$$\frac{d(PYR_a \times \delta(PYR_a))}{dt} = F_{PYRya} \times \delta(PYR_y) - pyrw_a \times \delta(PYR_a) - pyrdeg \times \delta(PYR_a) \quad (21)$$

Buried gypsum S (young):

$$\frac{d(GYP_y \times \delta(GYP_y))}{dt} = mgsb \times \delta(S) - gypw_y \times \delta(GYP_y) - F_{GYPya} \times \delta(GYP_y) \quad (22)$$

564 Buried gypsum S (ancient):

565 $$\frac{d(GYP_a \times \delta(GYP_a))}{dt} = F_{GYPya} \times \delta(GYP_y) - gypw_a \times \delta(GYP_a) - gypdeg \times \delta(GYP_a)$$

566 (23)

567 **List of fluxes**

568 Temperature dependence of basalt weathering:

569 $$f_{Tbas} = e^{0.061(T-T_0)}\{1 + 0.038(T - T_0)\}^{0.65}$$

570 (24)

571 Temperature dependence of granite weathering:

572 $$f_{Tgran} = e^{0.072(T-T_0)}\{1 + 0.038(T - T_0)\}^{0.65}$$

573 (25)

574 Temperature dependence of carbonate weathering:

575 $$g_T = 1 + 0.087(T - T_0)$$

576 (26)

577 Pre-plant silicate weathering: $f_{preplant} = f_T \cdot \sqrt{RCO_2}$

578 (27)

579 Plant-assisted silicate weathering: $f_{plant} = f_T \cdot \left(\frac{2RCO_2}{1+RCO_2}\right)^{0.4}$

580 (28)

581 Pre-plant carbonate weathering: $g_{preplant} = g_T \cdot \sqrt{RCO_2}$

582 (29)

583 Plant-assisted carbonate weathering: $g_{plant} = g_T \cdot \left(\frac{2RCO_2}{1+RCO_2}\right)^{0.4}$

584 (30)

585 Climate forcing for silicates:

586 $f_{CO2} = f_{preplant}(1 - \min(VEG \cdot W)) + f_{plant} \cdot \min(VEG \cdot W)$

587 (31)

588 $f_{CO2gran}$ and f_{CO2bas} result from the f_{CO2} function with plant-weathering feedbacks using

589 f_{Tgran} and f_{Tbas} respectively.

590 Climate forcing for carbonates:

591 $g_{CO2} = g_{preplant}(1 - \min(VEG \cdot W)) + g_{plant} \cdot \min(VEG \cdot W)$

592 (32)

593 Vegetation feedback: $VEG = 2 \cdot E \cdot \frac{(CO_2 ppm - 10)}{(183.6 + CO_2 ppm - 10)} \cdot \left(1 - \left(\frac{(T - T_0)}{T}\right)^2\right) \cdot$

594 $\left(1.5 - 0.5(RO_2)\right) \cdot \frac{k_{fire}}{\left(k_{fire} - 1 + \max(586.2 O_2(atm) - 122.102, 0)\right)}$

595 (33)

596 Evolution of plants: $pevol = \left(k_{preplant} + \left(1 - k_{preplant}\right) \cdot W \cdot VEG\right)$

597 (34)

598 Basalt weathering: $basw = \%bas_0 \cdot k_{silw} \cdot f_{CO2bas} \cdot PG \cdot pevol \cdot BA$

599 (35)

600 Granite weathering:

601 $granw = (1 - \%bas_0) \cdot k_{silw} \cdot f_{CO2gran} \cdot PG \cdot U \cdot pevol \cdot GA$

602 (36)

603 Silicate weathering: $silw = basw + granw$

604 (37)

605 Carbonate weathering (young): $carbw_y = k_{carbwy} \cdot g_{CO2} \cdot PG \cdot U \cdot pevol \cdot LAC_{rel}$

606 (38)

Carbonate weathering (ancient): $carbw_a = k_{carbwa} \cdot g_{CO2} \cdot PG \cdot U \cdot pevol \cdot LAC_{rel}$ (39)

Oxidative weathering (young): $oxidw_y = k_{oxidwy} \cdot U \cdot \sqrt{RO_2}$ (40)

Oxidative weathering (ancient): $oxidw_y = k_{oxidwa} \cdot U \cdot \sqrt{RO_2}$ (41)

Transfer from C_y to C_a: $F_{Gya} = carbw_a - ccdeg$ (42)

Transfer from G_y to G_a: $F_{Gya} = oxidw_a - ocdeg$ (43)

Marine carbonate carbon burial: $mccb = silw + carbw$ (44)

Seafloor weathering is revised to include direct temperature dependence as with terrestrial basalt weathering. This assumes a direct relationship between surface temperature change and seafloor temperatures.

Seafloor weathering: $sfw = k_{sfw} \cdot D \cdot e^{0.061(T-T_0)}$ (45)

In COPSE, sulphur degassing is assumed to have the same controls as sulphur weathering, therefore the degassing terms are accounted for by larger weathering terms:

Pyrite sulphur weathering (young): $pyrw_y = k_{pyrwy} \cdot U \cdot \frac{PYR_y}{PYR_{y0}} \sqrt{RO_2}$ (46)

Pyrite sulphur weathering (ancient): $pyrw_a = k_{pyrwa} \cdot U \cdot \frac{PYR_a}{PYR_{a0}} \sqrt{RO_2}$

(47)

Gypsum sulphur weathering (young): $gypw = k_{gypw} \cdot U \cdot \frac{GYP_y}{GYP_{y0}} \cdot \frac{carbw}{carbw_0}$

(48)

Gypsum sulphur weathering (ancient): $gypw = k_{gypw} \cdot U \cdot \frac{GYP_a}{GYP_{a0}} \cdot \frac{carbw}{carbw_0}$

(49)

Transfer from GYP_y to GYP_a: $F_{GYPya} = gypw_a - gypdeg$

(50)

Transfer from PYR_y to PYR_a: $F_{PYRya} = pyrw_a - pyrdeg$

(51)

Gypsum sulphur burial: $mgsb = k_{mgsb} \cdot \frac{S}{S_0} \cdot \frac{CAL}{CAL_0}$

(52)

Organic carbon degassing: $ocdeg = k_{ocdeg} \left(\frac{G}{G_0}\right) \cdot D$

(53)

Carbonate carbon degassing: $ccdeg = k_{ccdeg} \left(\frac{C}{C_0}\right) \cdot D \cdot B$

(54)

Marine carbonate carbon burial: $mccb = silw + carbw$

(55)

Total organic carbon burial:

$$ocb = \frac{1}{\Delta B}\Big(carbw_y\left(\delta(A) - \delta\left(C_y\right)\right) + carbw_a\left(\delta(A) - \delta(C_a)\right) + oxidw_y\left(\delta(A) - \delta\left(G_y\right)\right) + oxidw_a\left(\delta(A) - \delta(G_a)\right) + ccdeg\left(\delta(A) - \delta(C_a)\right) + ocdeg\left(\delta(A) - \delta(G_a)\right)\Big)$$

(56)

Total pyrite sulphur burial:

$$pyrb = \frac{1}{\Delta S}\Big(gypw_y\left(\delta(S) - \delta\left(GYP_y\right)\right) + gypw_a\left(\delta(S) - \delta(GYP_a)\right) + pyrw_y\left(\delta(S) - \delta\left(PYR_y\right)\right) + pyrw_a\left(\delta(S) - \delta(PYR_a)\right) + gypdeg\left(\delta(S) - \delta(GYP_a)\right) + pyrdeg\left(\delta(S) - \delta(PYR_a)\right)\Big)$$

(57)

Other calculations:

Relative atmospheric O_2: $RO_2 = \frac{\frac{O}{O_0}}{\frac{O}{O_0} + k_{O2}}$

(58)

where $k_{O2} = 3.762$

Solar forcing: $S = \frac{S_0}{1 + 0.38\left(\frac{t}{\tau}\right)}$

(59) where $S_0 = 1368 Wm^{-2}$, $\tau = 4.55 \times 10^9$ years.

Present day values:		**Source:**
Marine organic carbon burial:	$k_{mocb} = 4.5 \times 10^{12}$ mol C yr^{-1}	COPSE
Pyrite sulphur burial:	$k_{mpsb} = 5.3 \times 10^{11}$ mol S yr^{-1}	COPSE
Gypsum sulphur burial:	$k_{mgsb} = 1 \times 10^{12}$ mol S yr^{-1}	COPSE
Silicate weathering:	$k_{silw} = 4.9 \times 10^{12}$ mol C yr^{-1}	for steady state

Seafloor weathering:	k_{sfw} = 1.75x10^{12} mol C yr^{-1}	Mills et al. (2014)	
Oxidative weathering (young):	k_{oxidwy}=7x10^{12} mol C yr^{-1}	COPSE	
Oxidative weathering (ancient):	k_{oxidwa}=7.75x10^{11} mol C yr^{-1}		
	COPSE		
Carbonate weathering (young):	k_{carbwy}=1.8x10^{13} mol C yr^{-1}		
	COPSE		
Carbonate weathering (ancient):	k_{carbwy}=2x10^{12} mol C yr^{-1}		
	COPSE		
Pyrite sulphur weathering (young):	k_{pyrw}=2.36x10^{11} mol S yr^{-1}		
	COPSE		
Pyrite sulphur weathering (ancient):	k_{pyrw}=2.9x10^{11} mol S yr^{-1}		
	COPSE		
Gypsum sulphur weathering (young)	k_{gypwy}=7.5x10^{11} mol S yr^{-1}		
	COPSE		
Gypsum sulphur weathering (ancient)	k_{gypwy}=2.5x10^{11} mol S yr^{-1}		
	COPSE		
Organic carbon degassing:	k_{ocdeg}=1.25x10^{12}mol C yr^{-1}		
	COPSE		
Carbonate carbon degassing:	k_{ccdeg}=6.65x10^{12}mol C yr^{-1}		
	COPSE		
Atmosphere and ocean CO_2:	A_0=3.193x10^{18} mol		
	COPSE		

Ocean sulphate:	$P_0=4x10^{19}$ mol
COPSE	
Atmosphere and ocean oxygen:	$O_0=3.7x10^{19}$ mol
COPSE	
Buried organic carbon:	$G_0=1.25x10^{21}$ mol
COPSE	
Buried carbonate carbon:	$C_0=6.6x10^{21}$ mol
COPSE	
Buried pyrite sulphur:	$PYR_0=1.8x10^{20}$mol
COPSE	
Buried gypsum sulphur:	$GYP_0=2x10^{20}$ mol
COPSE	
Forcings:	**Attributes:**
Solar forcing:	$S = \frac{S_0}{1+0.38\left(\frac{t}{\tau}\right)}$
	where S_0 = 1368Wm^{-2}, τ=4.55x10^9 years.
Relative global CO_2 degassing:	$D = 1$ for present day
Relative uplift rate:	$U = 1$ for present day
Evolution of land plants:	$E = 1$ for present day
Weathering effect of plant evolution:	$W = 1$ for present day
Carbonate burial depth:	$B = 1$ for present day
Relative basaltic area:	$BA = 1$ for present day
Relative total land area:	LA_{rel} = 1 for present day
Relative carbonate land area:	LAC_{rel} = 1 for present day

Relative granite area: $GA = LA - LAC - BA_{cont}$

where BA_{cont} is the total basaltic area on continents (i.e. total basaltic area minus island arc and ocean island contributions) and LA and LAC are the total land area and carbonate land area respectively, calculated by scaling the relative areas to the present day areas.

Paleogeographical runoff effect: $PG = 1$ for present day

Starting conditions

The model reservoir of ancient carbonates, C_a, is by far the largest store of carbon, therefore its assumed isotopic composition at the start of the model run will influence the relative carbon burial rates for this time. This parameter is set so that organic C burial rates and oxygen concentration return to present day values at the end of the run (0Ma). This requires $\delta(C_{astart}) = 1.16$ for the GEOCARB δ^{13}Cinput, and $\delta(C_{astart}) = -0.56$ for the GTS2012 input.

Model output

Figure A2 shows IMB-COPSE model output for 3 combinations of input parameters:

1) δ^{13}C and δ^{34}S inputs follow GEOCARBSULF. Shown in green.
2) δ^{13}C input follows GEOCARBSULF, δ^{34}S inputs follow Algeo et al., (2015). Shown in orange.
3) δ^{13}C input follows GTS2012 (Saltzman and Thomas, 2012), δ^{34}S inputs follow Algeo et al., (2015). Shown in red.

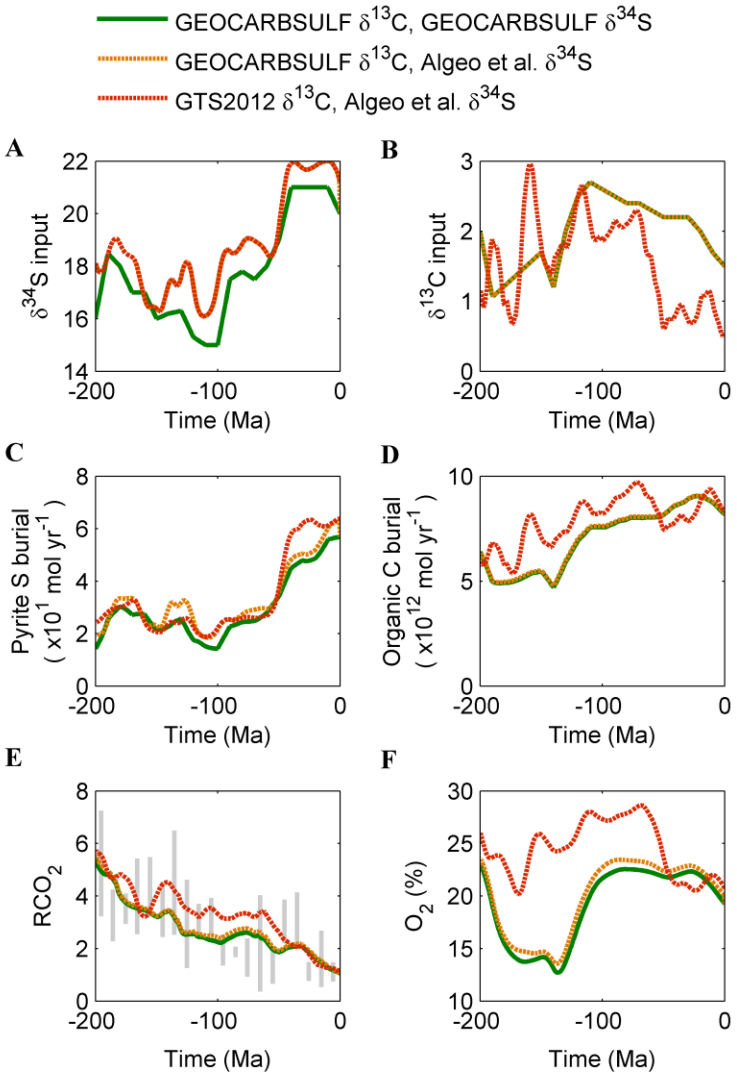

734

735 *Figure A2. IMB-COPSE model output for different isotope input scenarios. Relative*

736 *atmospheric CO_2 concentration plotted against compilation of Park and Royer (2011).*

737

738

739 Under the GEOCARBSULF inputs, the IMB-COPSE model predicts very similar

740 variations in atmospheric oxygen to the original GEOCARBSULF model (Berner, 2009;

741 see manuscript). When $\delta^{34}S$ input is altered to follow Algeo et al., (2015), oxygen

742 variation is only slightly affected, owing to the minor alteration to the input (around one

743 5th of the range), and to the significantly smaller fluxes of oxygen associated with the
744 sulphur system when compared to carbon. When the $\delta^{13}C$ input parameter is also altered,
745 predicted oxygen concentration is significantly changed, and is higher over the model
746 timeframe. This stems from the assumption that Mesozoic $\delta^{13}C$ was higher than present,
747 equating to greater organic carbon burial in this model variant.
748
749 **APPENDIX 3: ADDITIONAL MODEL EXPERIMENTS**
750 **Sensitivity of O_2 predictions to input parameters other than carbonate $\delta^{13}C$**
751 In the manuscript we show extreme sensitivity of modelled oxygen predictions to
752 carbonate $\delta^{13}C$ inputs. In figure A3 we test additional uncertainty by including error
753 estimates for other model processes. The grey area shows the extent of the range of
754 model predictions when run with $\pm 1\sigma$ variation in carbonate $\delta^{13}C$, but also with variation
755 between the minimum and maximum estimates for the rate of volcanic CO_2 degassing
756 and the global area of weatherable volcanic rocks. This mirrors the sensitivity window
757 shown in Mills et al., (2014). The effects on atmospheric oxygen predictions are minimal
758 when compared to the variation assumed in carbonate $\delta^{13}C$ alone (blue dashed lines). It
759 has been shown (Royer et al., 2014) that multi-parameter error analysis on all input
760 parameters (~70 for GEOCARBSULF) can result in similar uncertainty ranges for model
761 O_2 predictions as calculated here by varying only the $\delta^{13}C$ input. The grey error window
762 we show could be extended using this method (although many of these assumed error
763 windows are themselves arbitrary – the degassing rate and carbonate $\delta^{13}C$ curve used in
764 this modelling are significantly outside the error range used by Royer et al., (2014)), but
765 the median predictions are not altered by such analyses.

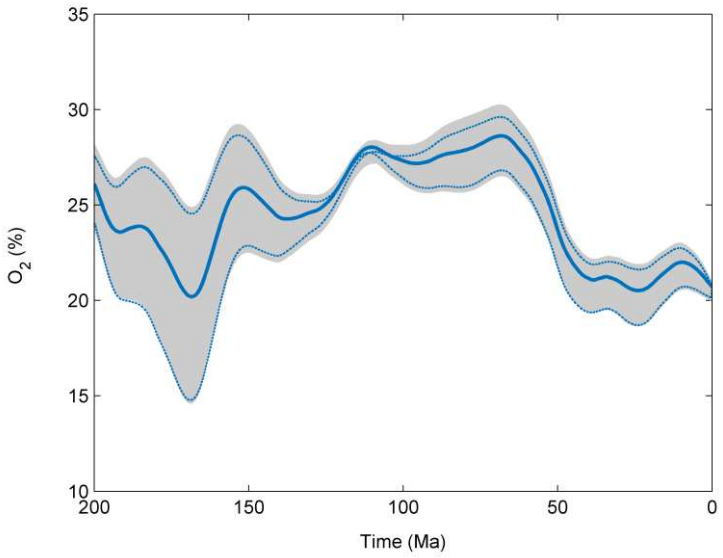

Figure A3. Model error window (grey) when subject to max/min variation in inputs for carbonate $\delta^{13}C$, volcanic CO_2 degassing rate and weatherable area of volcanic rocks. See Mills et al., (2014) for details of these processes. Compared to model error window under $\pm 1\sigma$ in carbonate $\delta^{13}C$ input (blue dashed lines).

Model sensitivity to carbonate reservoir variations.

Our model assumes an increase in the degassing rate of carbonates at ~140Ma, aiming to represent the subduction of deep ocean carbonate deposits after the evolution of calcareous plankton (burial depth forcing *B* above, following from GEOCARB modelling). However, carbonate subduction may be more dependent on longer term basin dynamics and may therefore produce a destabilizing effect on the carbon cycle (Edmond and Huh, 2003). In figure A4 we replace the *B* forcing with a new flux from the young carbonate reservoir to the atmosphere/ocean. This represents tectonic control of carbonate subduction and follows Edmond and Huh (2003; panel A). As discussed by these authors, this flux can have a considerable impact on model CO_2 predictions. This follows from the

idea that the modern day steady state does not include some significant past processes. The impact on our oxygen predictions is however relatively small: the increase in carbon fluxes only represents around 10% of the total gross throughput, and therefore does not greatly alter the mass balance calculation or O_2 (see manuscript).

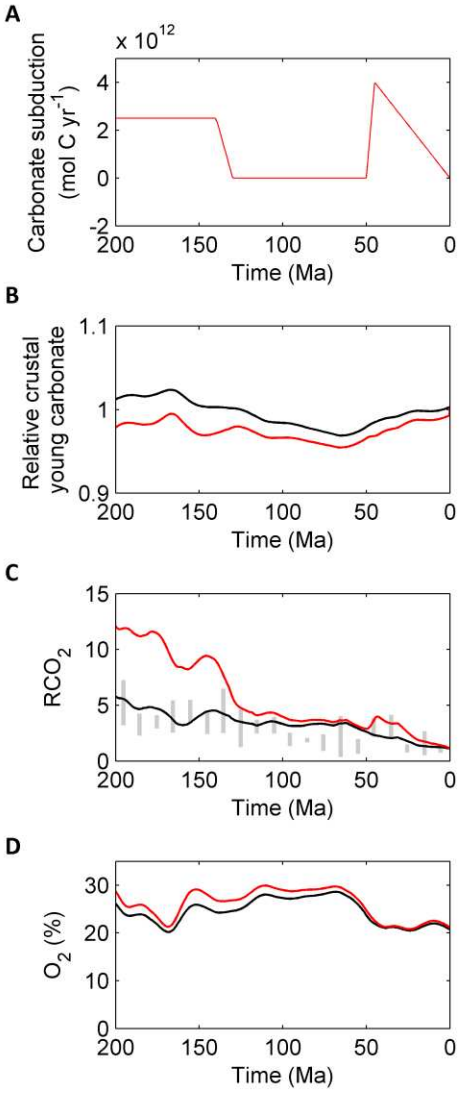

Figure A4. Model configured with additional carbonate subduction flux from young carbonates to atmosphere/ocean (red). Compared to original model (black).

Model sensitivity to pyrite burial constraints.

The quantity f_{pyr} represents pyrite burial as a fraction of total sulphur burial. In GEOCARB and COPSE modelling f_{pyr} is around 0.3-0.4 at the present day. It has however been suggested, based on direct estimation of the sulphate burial rate, that f_{pyr} may have been as high as 0.9 and stable at this fraction for the whole Phanerozoic (Halevy et al., 2012). To close the isotope mass balance under this constraint requires a fixed time-evolution of the isotopic composition of sulphate inputs (figure A5, panel A), although this is not supported by available data on the composition of sulphur in coals (Canfield, 2013). In figure A5 we run the model with an imposed $\delta^{34}S$ of sulphate inputs, and an increased rate of pyrite burial at present day (Halevy et al., 2012). Variation in oxygen predictions are again small. This is because the rate of oxygen production from pyrite burial is still much smaller than via organic carbon burial (around 20%), and also because the higher and more stable rate of pyrite burial in the altered model acts to reduce the overall variation in oxygen production rates.

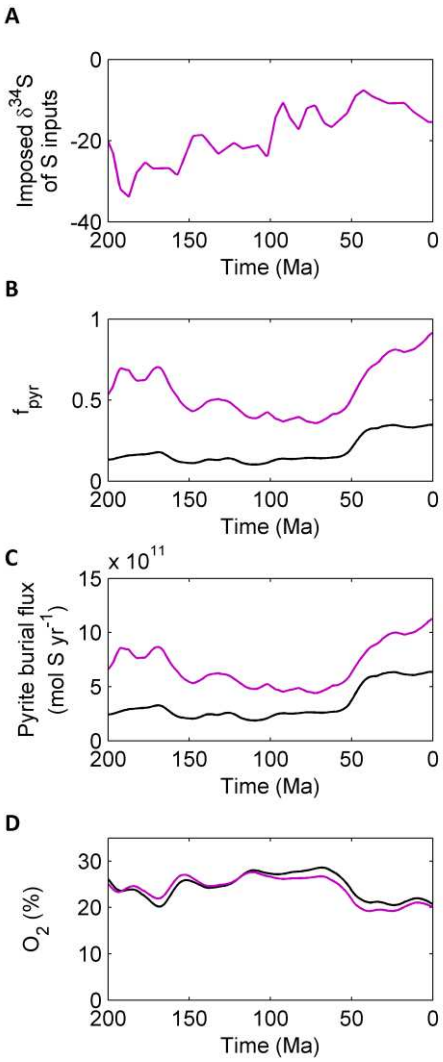

Figure A5. Model configured with higher rate of pyrite burial and imposed $\delta^{34}S$ value for sulphate inputs (purple). Compared to original model (black).

ADDITIONAL REFERENCES

Berner, R. A., 1991, A model for atmospheric CO_2 over Phanerozoic time: American Journal of Science, v. 291, p. 339-376.

Berner, R. A., 1994, Geocarb II: A revised model of atmospheric CO_2 over Phanerozoic time: American Journal of Science, v. 294, p. 56-91.

814 Berner, R. A., and Kothavala, Z., 2001, Geocarb III: A revised model of atmospheric CO_2
815 over Phanerozoic time: American Journal of Science, v. 301, p. 182-204.
816 Canfield, D. E., 2013, Sulfur isotopes in coal constrain the evolution of the Phanerozoic
817 sulfur cycle. PNAS v. 110, p. 8443-8446.
818 Edmond, J. M. and Huh, Y., 2003, Non-steady state carbonate recycling and implications
819 for the evolution of atmospheric pCO_2. EPSL v. 216, p. 125-139.
820 Halevy I, Peters S. E. and Fischer W. W., 2012, Sulfate burial constraints on the
821 Phanerozoic sulfur cycle. Science v. 337, p. 331–334.
822 Park, J., and Royer, D. L., 2011, Geologic constraints on the glacial amplification of
823 Phanerozoic climate sensitivity: American Journal of Science, v. 311, p. 1-26.